Coherent Raman beats: high-order interference effects

Dieter Suter and Thomas Marty

Institute of Quantum Electronics, Swiss Federal Institute of Technology Zürich, CH-8093 Zürich, Switzerland

Received March 8, 1993

Light propagating through an optically anisotropic resonant medium excites coherent Raman fields that propagate together with the original wave; the interference between the two fields generates the well-known Raman beats. We solve the coupled-wave equations for finite optical path lengths and show how the coherent exchange of energy between the two fields leads to interference effects that distort the observed signal for different detection schemes. Theoretical analysis is compared with experimental results from the Na D_1 transition.

Stimulated Raman scattering can be understood as a coupling between the laser and Raman waves and a coherent excitation of the resonant medium oscillating at the difference between the two optical frequencies.[1] Coherent Raman scattering is a modification where a coherent excitation, which is already present in the medium, enhances the coupling between the laser and Raman waves. Under these conditions the laser beam excites a Raman field in first order in the incident field, and the Raman mode contains equal amounts of Stokes and anti-Stokes components.[2] Continuous experiments of this type usually excite this superposition state through a radio-frequency[3,4] or microwave field,[5,6] whereas transient experiments include the use of laser pulses,[7] frequency switching of the laser,[8] and Stark switching of the molecular resonance frequency[9–11] to prepare the medium in an anisotropic state before the actual Raman process takes place. In many cases of practical interest the Raman-shifted field propagates parallel to the laser field. If the two fields interfere on the detector, the resultant Raman beats[10,12] contain information about the frequency shift and the relative amplitude of the Raman field. This procedure not only results in high sensitivity, but the observed beat signal is also unaffected by Doppler broadening, optical dephasing, and laser frequency fluctuations. The method is therefore ideally suited for spectroscopic applications such as the determination of ground-state relaxation rates.[13]

In the observations of coherent Raman beats reported so far the amplitude of the scattered field was always much smaller than that of the unshifted beam, so that the theoretical description could safely neglect changes in the amplitude of the laser field. However, typical experimental conditions can easily lead to Raman amplitudes comparable with the amplitude of the laser field. Although such conditions maximize signal intensity, they can significantly complicate data analysis. In this Letter we treat this case explicitly by discussing the propagation of the coupled laser and Raman waves. We do not discuss the excitation of the medium but assume that a laser pulse has created a coherent superposition of ground-state sublevels before the actual Raman process.[14] In the atomic system that we use in our experimental example, the ground state of atomic sodium, only the coherences ρ_{rs} between neighboring Zeeman substates ($r - s = \pm 1$) contribute to the observed signal. The six possible sublevel transitions of this type have transition frequencies ω_{rs}, which are roughly proportional to the magnetic field (~7 MHz/mT) but differ slightly owing to quadratic Zeeman and nuclear Zeeman effects.

Because the wavelength of the sublevel transition is much larger than the sample size, we do not have to consider phase matching. Figure 1 summarizes the processes that contribute to the Raman scattering. The curved arrows indicate sublevel coherences ρ_{rs}, and the straight lines indicate the interaction with the incident light that may be σ or π polarized. Coupling of the light to the ground-state sublevel coherences excites polarization in the optical transitions, which are marked by the wavy lines. Obviously, the scattering process is associated with a change in polarization of the light: incident σ light excites π-polarized optical coherences and vice versa.

We calculate the resulting propagation effects starting from Maxwell's wave equation $\partial E_i/\partial x = -2\pi i k P_i$, where E_i indicates the slowly varying field amplitude of polarization i, P_i is the corresponding polarization of the medium, k the optical wave vector, and x is the propagation length. To first order in the incident field, we get two simple equations for the wave propagation:

$$\frac{\partial E_\parallel}{\partial x} = -c_{\mathrm{tot}}(t) E_\perp , \qquad \frac{\partial E_\perp}{\partial x} = c_{\mathrm{tot}}(t) E_\parallel , \tag{1}$$

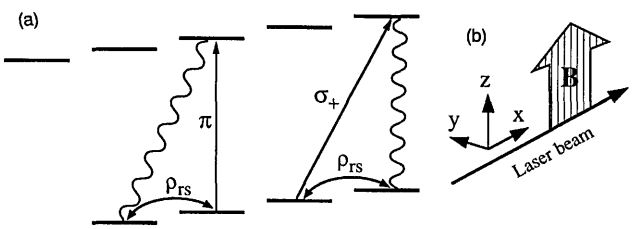

Fig. 1. Schematic representation of the Raman-scattering processes. For simplicity, only the two $F = 2$ multiplets of the Na D_1 transition are shown. The curved arrows indicate two ground-state coherences, the solid lines represent the incident light, and the wavy lines mark the resulting optical polarization. (b) Relevant geometry and choice of coordinate system.

0146-9592/93/191663-03$6.00/0 © 1993 Optical Society of America

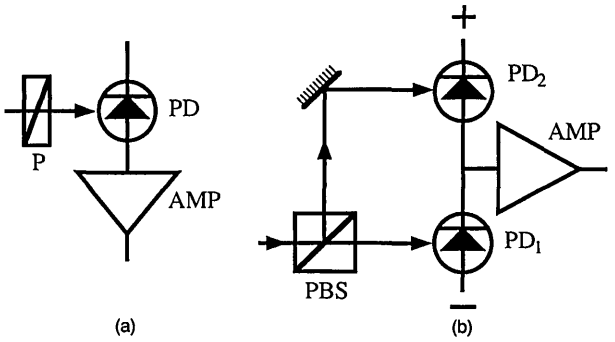

Fig. 2. Schematic representation of the detection setup for (a) conventional heterodyne detection and (b) balanced heterodyne detection. P, polarizer; PBS, polarizing beam splitter; PD's, photodiode's; AMP, amplifier.

where the subscripts $\|$ and $\perp$ refer to the polarization components parallel and perpendicular, respectively, to that of the incident beam. In the case of atomic Na the coupling constant $c_{tot}(t)$ includes contributions from all six sublevel coherences:

$$c_{tot}(t) = c_0\,\mathrm{Re}[\rho_{12}(t) + \rho_{23}(t) + 2\rho_{45}(t) + 3\rho_{56}(t) + 3\rho_{67}(t) + 2\rho_{78}(t)]. \quad (2)$$

Here the first two coherences are between Zeeman sublevels of the $F = 1$ multiplet, and the other four coherences are in the $F = 2$ multiplet; the constant c_0 is proportional to the transition strength and the particle density. Equations (1) have the obvious solutions

$$E_{\|} = E_0 \cos(c_{tot}\, x), \qquad E_{\perp} = E_0 \sin(c_{tot}\, x), \quad (3)$$

where E_0 represents the amplitude of the incident field. The Raman field therefore contains Stokes and anti-Stokes modes with equal amplitudes and linear in the exciting field, as is generally the case with coherent Raman scattering.[2]

Before detecting the resulting signal, one has to select a polarization component, as shown in Fig. 2(a). If this polarizer is oriented parallel to the polarization of the incident laser field, the resulting signal is $S_0 = |E_{\|}|^2 = E_0^2 \cos^2(c_{tot}\, l)$, valid for arbitrary sample length l. For small optical path lengths $c_{tot}\, l$, this can be expanded as $S_0 = E_0^2(1 - c_{tot}^2\, l^2 + \ldots)$. Thus, the unshifted laser field dominates the signal, whereas the Raman contribution enters only in second order. If several Raman transitions are present, we expect to find sums and differences of all sublevel frequencies. With the polarizer in the orthogonal orientation, we measured the complementary signal $S_{90} = E_0^2(c_{tot}^2\, l^2 - \ldots)$. In this case the different components of the Raman field interfere with each other; the observed frequencies are again sums and differences of the Raman frequencies.

In the usual heterodyne detection the analyzer is oriented at an intermediate angle, typically $\pm\pi/4$, and the Raman field beats against the laser field. The signal is then $S_{\pm 45} = (1/2)|E_{\|} \pm E_{\perp}|^2$. The difference between these two signals, $S_{45} = S_{+45} - S_{-45} = E_0^2 \sin(2c_{tot}\, l)$, provides an even more useful quantity; a possible experimental setup is shown in Fig. 2(b). This signal can again be expanded as $S_{45} = 2E_0^2[c_{tot}\, l - (2/3)c_{tot}^3\, l^3 + \ldots]$. In the limit of small Raman intensity this scheme corresponds to a direct measurement of the Raman amplitude; in the ideal case it is insensitive to fluctuations of the laser frequency and amplitude, in close analogy to balanced heterodyne detection.[15] In terms of the density operator elements of the Na ground state, the first-order signal is

$$S_{45}^{(1)} = l c_0\,\mathrm{Re}(\rho_{12} + \rho_{23} + 2\rho_{45} + 3\rho_{56} + 3\rho_{67} + 2\rho_{78}). \quad (4)$$

The different sublevel coherences therefore contribute linearly to the total signal. If they precess at different frequencies, $\rho_{rs}(t) = \rho_{rs}(0)\exp(i\omega_{rs}t)$, their contributions to the signal can be separated by Fourier transformation. The next higher order is proportional to the third power of the optical path length and contains triple products of the density operator elements. If these elements evolve at a single frequency ω_0, the resulting signal contribution contains frequency components at ω_0 and $3\omega_0$; in general the signal contains contributions that evolve at frequencies $(\pm\omega_{rs} \pm \omega_{r's'} \pm \omega_{r''s''})$, i.e., algebraic sums of three precession frequencies.

We compared these predictions with measurements performed on the $3s^2S_{1/2}$ Na ground state. A 4-cm-long glass cell contained the atomic vapor, together with 200 mbars of Ar buffer gas. The laser frequency was set near the Na D_1 line ($\lambda = 589.6$ nm) with a detuning $\Delta = 15$ GHz above the center of the resonance line. A circularly polarized laser pulse, derived from the same laser, excited the sublevel coherences, and the Raman signal was observed after the pump pulse was switched off.[14] The probe laser beam was linearly polarized and had an intensity of $\sim 100\ \mu\mathrm{W/mm^2}$.

A first experiment was performed in a transverse field of 15 μT, where the precession frequency of all

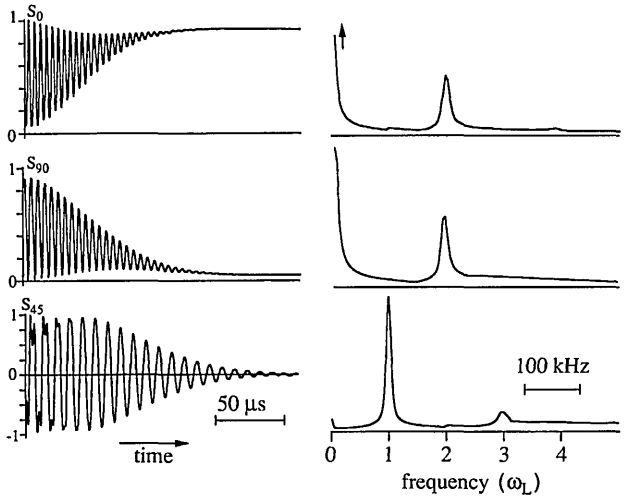

Fig. 3. Experimental signals observed in the case of a single Raman frequency. The left-hand column contains time-domain data for the analyzer oriented parallel (top) and perpendicular (center) to the polarization of the incident beam. The signal at the bottom was recorded with the balanced heterodyne detection scheme of Fig. 2(b). The Raman spectra in the right-hand column were obtained by Fourier transformation of the time-domain data.

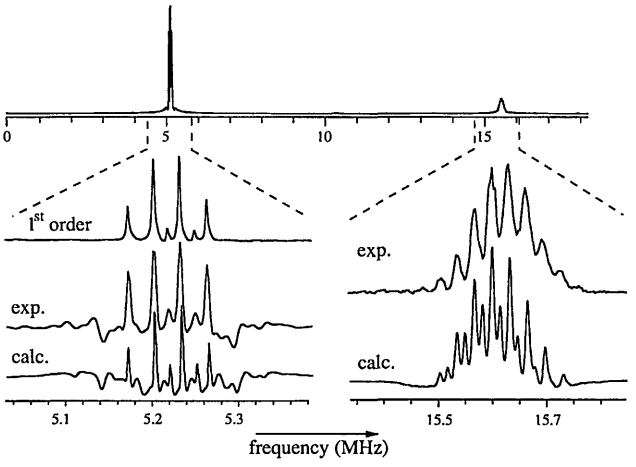

Fig. 4. Experimental signal observed for the case of multiple sublevel frequencies: the upper trace shows the complete Raman spectrum, and the lower traces contain expansions of the regions close to the first and third harmonics of the Larmor frequency.

six sublevel coherences is close to 100 kHz. Figure 3 compares the resulting signals for different orientations of the analyzer. The data were recorded at a particle density where the optical path length $c_{tot}\, l$ is on the order of 1, which results in an almost complete exchange of energy between the two orthogonal polarizations. The left-hand column contains the Raman beat signal, and the right-hand column shows the Fourier transforms of the time-domain data. The signal in the top row was recorded with the analyzer parallel to the polarization of the incident laser light. The Raman spectrum shows clearly that only the even harmonics of the Larmor frequency are present; the relative heights of the two contributions depend on the optical path length, which can be controlled experimentally through the particle density. The signal in the center row was recorded with the analyzer in the orthogonal orientation. It contains the complement of the top row signal and therefore consists of the same frequency components. The signal in the bottom row was recorded with the balanced heterodyne detection scheme of Fig. 2(b). In this case the first and third harmonics of the Larmor frequency dominate the signal.

Figure 4 shows data recorded in a transverse magnetic field of 0.74 mT. At this field strength, the quadratic Zeeman and the nuclear Zeeman effect make all six precession frequencies distinguishable. The top row shows the Raman spectrum, which was obtained with the balanced heterodyne detection scheme of Fig. 2(b). The spectra in the lower part of the figure contain expansions of the regions close to the first and third harmonics of the Larmor frequency. In the region near 5.2 MHz the low-order signal contains only the clearly identifiable signal contributions from the six sublevel coherences, as predicted by Eq. (4). The two lower spectra contain the experimental and calculated spectra for higher densities, where additional frequency components appear that correspond to algebraic sums of three or more precession frequencies. If all three frequencies appearing in these sums have the same sign, the observed frequency is close to 15.6 MHz. If one of the signs differs, the signal appears in the region near 5.2 MHz. Even in third order there are several hundred frequencies contributing to the overall signal; therefore a full analysis of such a high-order spectrum becomes an extremely time-consuming task.

In conclusion, we have discussed the effect of finite optical path lengths in coherent Raman-scattering experiments. The coherent exchange of energy between the two waves can be observed as multiple Raman scattering and, in the case of distinguishable Raman transitions, as interferences between different contributions to the total signal. Depending on the detection geometry, it is possible to select the even or odd harmonics of the Raman signal. We used experimental examples from the Na ground state to illustrate the theoretical results, which are completely general and may be applied to other systems. Experimental conditions that cause multiple Raman scattering, as in our example, may be useful for generating frequency-shifted light, if only a single Raman process contributes. If different Raman frequencies contribute, however, the many frequency components that contribute to higher-order signals result in a spread of signal energy that can significantly complicate the analysis of the observed data.

This work was supported by the Schweizerischer Nationalfonds.

References

1. R. W. Hellwarth, Phys. Rev. **130,** 850 (1963).
2. J. A. Giordmaine and W. Kaiser, Phys. Rev. **144,** 676 (1966).
3. J. Mlynek, N. C. Wong, R. G. DeVoe, E. S. Kintzer, and R. G. Brewer, Phys. Rev. Lett. **50,** 993 (1983).
4. M. Mitsunaga, E. S. Kintzer, and R. G. Brewer, Phys. Rev. B **31,** 6947 (1984).
5. N. Bloembergen, P. S. Pershan, and L. R. Wilcox, Phys. Rev. **120,** 2014 (1960).
6. K. Holliday, X. F. He, P. T. Fisk, and N. B. Manson, Opt. Lett. **15,** 983 (1990).
7. M. Bassini, F. Biraben, B. Cagnac, and G. Grynberg, Opt. Commun. **21,** 263 (1977).
8. R. G. Brewer and A. Z. Genack, Phys. Rev. Lett. **36,** 959 (1976).
9. R. L. Shoemaker and R. G. Brewer, Phys. Rev. Lett. **28,** 1430 (1972).
10. R. G. Brewer and E. L. Hahn, Phys. Rev. A **8,** 464 (1973).
11. E. W. Van Stryland and R. L. Shoemaker, Phys. Rev. A **20,** 1376 (1979).
12. N. C. Wong, E. S. Kintzer, J. Mlynek, R. G. DeVoe, and R. G. Brewer, Phys. Rev. B **28,** 4993 (1983).
13. R. J. McLean, P. Hannaford, and R. M. Lowe, Phys. Rev. A **42,** 6616 (1990).
14. D. Suter and J. Mlynek, Adv. Magn. Opt. Reson. **16,** 1 (1991).
15. H. P. Yuen and V. W. S. Chan, Opt. Lett. **8,** 177 (1983).